Evolution of the structural and magnetic properties of sputtered $Tb_xFe_{73}Ga_{27-x}$ (7 at.% ≤ x ≤ 11 at.%) thin films upon the increase of Tb content

R. Ranchal[1], S. Fin[2], and D. Bisero[3]

[1]*Dpto. Física de Materiales, Facultad de Ciencias Físicas. Universidad Complutense de Madrid. Ciudad Universitaria s/n, Madrid 28040, Spain*

[2]*Dipartimento di Fisica, Università di Ferrara, Via Saragat 1, 44122 Ferrara, Italy*

[3]*CNISM and Dipartimento di Fisica, Università di Ferrara, Via Saragat 1, 44122 Ferrara, Italy*

Abstract

$Tb_xFe_{73}Ga_{27-x}$ (7 at.% ≤ x ≤ 11 at.%) ternary alloys have been obtained by cosputtering from $Tb_{33}Fe_{67}$ and $Fe_{72}Ga_{28}$ targets. In contrast with other Tb-Fe-Ga compounds that consist of just one structural phase, the diffraction pattern of the $Tb_7Fe_{73}Ga_{20}$ shows the presence of two different phases related to binary Tb-Fe and Fe-Ga alloys. This microstructure evolves as the Tb content is increased, and for a Tb of 11 at.% x-ray diffractometry only evidences the presence of a phase close to the $TbFe_2$. Although none of the studied samples show perpendicular magnetic anisotropy, there is a significant component of the magnetization perpendicular to the sample plane. The increase of the Tb content on the compounds from 7 at.% to 11 at.% enhances this component most probably due to the shift of the microstructure towards one similar to the $TbFe_2$.

1. Introduction

Magnetic thin films exhibit a close correlation between structural and magnetic properties being possible to tailor their magnetic characteristics by means of the growth conditions. In the last years, $Fe_{1-x}Ga_x$ alloys have received great attention due to their unique magnetoelastic properties [1-10]. The magnetostriction constant (λ_s) for these alloys shows two peaks for Ga contents of 18 at.% and 29 at.% [8]. The exact position of these peaks depends on the thermal history during processing being achieved higher magnetostriction values in quenched samples [8]. The largest λ_s value is observed in the (100) direction also reflecting the strong correlation between structural and magnetoelastic properties in this material system. Nevertheless, $Fe_{1-x}Ga_x$ compounds exhibit a tendency to the (110) texture when deposited in form of thin films either by electrodeposition or vacuum techniques [11-15]. $TbFe_2$ has also been deeply studied due to its huge λ_s of around 4000 ppm at 10 K and 2500 ppm at room temperature [16]. Also, it has been reported perpendicular magnetic anisotropy (PMA) in $TbFe_2$ and the influence of growth conditions and composition on it [17-19]. Nevertheless, its high coercivity and brittleness have reduced the interest on this material system.

Recently, it has been reported the increase of λ_s in Fe-Ga alloys with a Ga content ~ 17 at.% doped with a quantity of Tb below 1 at.% [20-23]. In particular, λ_s shows an increase of ~ 250 % in (110)-textured polycrystalline alloys doped with a 0.3 at.% of Tb [23]. Besides, there have also appeared works about ternary Tb-Fe-Ga compounds where another compositional range has been explored, $Tb_yFe_{100-x-y}Ga_x$ thin films with y between 9 and 10 at.% and x from 13 to 16 at.% obtained by cosputtering [24-25]. The magnetic anisotropy and the possibility to control it by means of the growth conditions have been the main goal of those studies. Although PMA has been observed for some specific compositions, the compositional range and the growth conditions analyzed so far are rather small. One of the main differences between the ternary compounds studied so far is the microstructure. When the Tb content is low (below 1 at.%), the compound exhibits a bcc structure similar to what is found in Fe-Ga alloys [20]. When the Tb content is higher, around 10 at.%, the microstructure is closer to that of $TbFe_2$ [24]. Nevertheless, more studies are necessary to know the microstructure and magnetic behavior in each compositional range. In addition, it is of relevance the investigation of the effect of growth conditions as already indicated by previous works [25]. Here, we present an investigation about the magnetic behavior of

$Tb_xFe_{73}Ga_{27-x}$ (7 at.% ≤ x ≤ 11 at.%) thin films obtained by cosputtering. In comparison to previous works, we have analyzed alloys deposited at a lower distance between target and substrate and with the same type of power source (DC) in both targets. We have observed an evolution of the microstructure from two to one phase as the Tb content is increased from 7 at.% to 11 at.%. We have also studied the out-of-plane (OOP) component of the magnetization and its dependence with the structural properties.

2. Experimental techniques

Samples were deposited at room temperature on 5 × 4 mm^2 glass substrates. Two targets with a nominal composition of $Tb_{33}Fe_{67}$ and $Fe_{72}Ga_{28}$ were employed to cosputter the alloys. The targets have a diameter of 5 cm and a thickness of 0.3 cm. The deposition was performed in the oblique incidence, being the angle of incidence between each target and the substrate of about 25° and the distance between the targets and the substrate of 9 cm, i.e., smaller than in previous works [24-25]. Another difference in comparison to previous works is the use of a DC power source in the two targets. Before the deposition of each sample, the base pressure was below 4×10^{-7} mbar. To obtain samples with different compositions, we have kept fixed a power of 90 W in the $Fe_{72}Ga_{28}$ being modified between 50 and 90 W in the $Tb_{33}Fe_{67}$ target. The growth rate was calibrated in previous samples measuring the thickness of the layers as described in [26]. Then, the time of deposition was controlled to obtain a thickness of around 320 nm in the layers shown in this work. Mo 20 nm thick was used as buffer and capping layers for all the samples. They were grown with a DC power of 90 W. The Ar pressure was 2×10^{-3} mbar to evaporate all the layers: buffer, capping, and ternary Tb-Fe-Ga alloys.

We have focused our attention on the analysis of as-grown samples, i.e., we have not performed any thermal treatment previous to the analysis of the samples. The composition of the samples was analyzed by means of the Energy Dispersive X-ray Spectroscopy (EDS) in a JEOL JSM 7600F SEM microscope operated at 20 kV and 9 μA. We have estimated an uncertainty of around 1 at.% in the compositional measurements. θ-2θ x-ray diffractometry (XRD) patterns were measured in the Bragg-Brentano configuration. The step size of the diffraction scans (0.02°) was optimized considering that the layers are polycrystalline with diffraction peaks rather wide. At room temperature, in-plane and out-of-plane hysteresis loops were carried out in a

vibrating sample magnetometer (VSM). In the VSM we can rotate the sample being possible to measure the in-plane loops at different angles between the applied magnetic field and the in-plane reference direction, the long side of the substrates. The same routine as in previous works was used for the field-cooled (FC) curves performed in a superconducting quantum interference device (SQUID) magnetometer [24]. Prior to measuring the temperature dependence of the magnetization, the sample was first cooled from room temperature to 5 K under a saturation field of 2 kOe and then, the FC curves were recorded with an applied magnetic field of 100 Oe during the warming-up. Hysteresis loops at 10 K were also performed in the SQUID magnetometer. Magnetic Force Microscopy (MFM) images were recorded by a Digital Instruments Nanoscope IIIa, using the phase detection mode, i.e., monitoring the cantilever's phase of oscillation while the magnetic tip was scanning the sample surface at a distance of 80 nm on the average (lift mode). Commercially available ferromagnetic CoCr tips were used. The MFM measurements were performed both at remanence and in-field (applying an external magnetic field lying in the plane of the film, with an intensity of 0.8 kOe) [27-28]. In order to exclude the influence of the tip on the magnetic state of the sample, we used different scanning directions and tip to sample distances, obtaining the same results with different operating conditions.

3. Results and discussion

Our experimental results show that the composition of the alloys can be controlled by means of the growth power applied in the $TbFe_2$ target (table I). Thanks to the growth conditions proposed in this work, we have managed to keep fixed the Fe content in the 73 at.%. The increase of the growth power in the $TbFe_2$ target from 50 W to 90 W modifies the Tb from 7 to 11 at.% as the Ga is reduced from 20 to the 16 at.% (table I). When the atoms ejected from the targets arrive to the substrate, they suffer resputtering and reflection processes [29-30]. All these processes can affect the composition of the layers because each type of atom can suffer a different resputtering or reflection phenomena. This fact can explain that the Tb-Fe-Ga ternary compounds have an Fe content of 73 at.% in spite of starting with targets with a lower Fe content. We have analyzed the structure of the samples by means of x-ray diffractometry (figure 1). We also present the diffraction pattern of a Mo layer deposited in the same way as the buffer and capping layers for a better analysis of the results. The peak at $2\theta \sim 73.68°$ corresponds to the reflection (211) of Mo. In the samples studied in this work, it is

observed a diffraction peak at 40.7° as also observed in previous works about Tb-Fe-Ga compounds with a Tb content ~ 10 at.% [24-25]. Although this peak is near the (110) of Mo, it is closer to that of the $TbFe_2$ being possible to correlate it to the latter structure (Fig. 1b). In addition to the reflection at 40.7°, XRD also evidences a second peak around 44°. The theoretical value for α-Fe is $2\theta = 44.67°$, but it moves towards lower angles as Ga is introduced in the Fe lattice and it can appear at $2\theta = 44.1°$ for a Ga content of 25 at.% [9]. In our samples, we find the α-Fe (110) reflection below 44°, which points to the formation of $Fe_{1-x}Ga_x$ alloys with a Ga content higher than 25 at.%. The existence of this reflection indicates a disordered A2 phase with a (110) texture as generally observed in Fe-Ga thin films [12-15]. It can also be observed that the position of this diffraction peak (related to Fe-Ga compounds) depends on the Tb content. It moves to smaller diffraction angles and decreases its intensity as it is raised the content of Tb in the samples (Fig. 1b). These two effects can be explained by considering the introduction of Tb in the Fe-Ga matrix as recently reported by Ma et al. [20]. On one hand, the introduction of Tb in the Fe-Ga matrix increases its lattice parameter because of the larger atomic radius of Tb and on the other, the disorder promoted in the Fe-Ga matrix by the Tb introduction reduces the intensity of the diffraction peak related to the Fe-Ga alloys present in the samples. In bulk samples obtained by other preparation techniques it has been reported a solubility limit of 0.2 at.% for Tb in the A2 phase of Fe-Ga [22-23]. In our compounds the Tb content is higher than that solubility limit, and in agreement with those reports, we observe a phase separation as indicated by the presence of diffraction peaks related to both Fe-Ga and Tb-Fe alloys. However, for a Tb content of 11 at.% ($Tb_{11}Fe_{73}Ga_{16}$), XRD only evidences the presence of one structural phase similar to $TbFe_2$ (Fig. 1b) as reported in previous works in which much higher Tb dopings are introduced [24-25]. Therefore, the growth conditions proposed in this work enable to tune the structure of $Tb_xFe_{73}Ga_{27-x}$ ($7 \text{ at.\%} \leq x \leq 11 \text{ at.\%}$) thin films from two separate phases, related to Fe-Ga and Tb-Fe alloys, to one phase similar to $TbFe_2$ as the Tb content increases from 7 at.% to 11 at.%.

We have analyzed the magnetic properties measuring the hysteresis loops with the applied magnetic field in and perpendicular to the sample plane (Fig. 2). A sample will show PMA if two conditions are fulfilled: a) it is magnetically isotropic in the sample plane, i.e. there is no difference between the hysteresis loops measured at different angles between the in-plane magnetic field and the reference direction, and b)

the OOP direction is an easy axis in comparison to any direction in the sample plane. Regardless of the composition, we have found that the OOP direction is not an easy axis in none of the studied samples (Fig. 2) and therefore, there is not a clear PMA in the samples studied in this work.

The absence of PMA does not rule out the existence of a significant stray field emerging from the plane of the sample in the perpendicular direction. As a matter of fact, we observe a clear OOP component by MFM, as demonstrated by Figure 3, where the image at remanence corresponding to the sample with a Tb content of 10 at.% is reported and compared with the AFM image. In order to exclude the correlation between magnetic and topographic signals the comparison of relevant magnetic structures with the corresponding topographic reference is shown in figure 3. In particular, similar morphological textures detected by AFM (compare the three circular and the two elliptical highlighted zones) lead to very different magnetic structures. The surface roughness of the film, as determined by the AFM image reported in figure 3, is 5 nm and the Power Spectral Density function (based on the Fourier analysis of the MFM micrograph) is greater than 50 nm (figure 3c): this means that the dimension of magnetic domains is one order of magnitude greater than the roughness of topography. The value of roughness is much lower than the lift height (80 nm) used in the MFM measurements and this avoid an influence of the topography in the detection of MFM signal. Moreover a direct comparison of the AFM profile of a specific section with the correspondent MFM profile (3d, 3e)definitely confirm the uncorrelation between the two signals [31-32]. The results shown in figure 3 must be considered as representative of the magnetic signal observed in all the analyzed samples. The image consists of magnetic structures which are not modified in their overall shape and dimension by the presence of an external in-plane field up to 800 Oe. The shape of the magnetic structures and their in-field stability is comparable to the ones observed in samples [33], where the OOP component was detected and studied. In a previous study on Tb-Fe-Ga compounds with similar Tb but lower Ga content [25], we showed that the stability of the magnetic domains was more related to the power source used during deposition than to the composition of the alloy. For a composition of $Tb_{10}Fe_{76}Ga_{14}$, there were obtained more stable magnetic domains and a higher PMA when using a DC power supply in the $TbFe_2$ target. In this work, we have used DC power sources in the two targets and a smaller target to substrate distance. With these growth conditions, we have managed to

obtain stable magnetic structures with an OOP magnetization even in layers comprised of two separate phases (figure 3).

In figure 4 (a) we present a detail of the hysteresis loops recorded with the magnetic field in the perpendicular direction. It is clear that the increase of Tb in the compound enhances the OOP component of the magnetization. The hysteresis loop of the sample with the lowest Tb content (7 at.%) does not saturate for the maximum applied magnetic field of 12.5 kOe. However, the hysteresis loops modify their shape as the Tb content is increased and eventually for a Tb of 11 at.%, the loop saturates for a magnetic field of a little bit less of 12.5 kOe. It is important to remark that the $Tb_{11}Fe_{73}Ga_{16}$ layer does not present an easy axis in the OOP direction but an enhancement of the magnetization component in that direction in comparison to the other samples. We can correlate the shape of these perpendicular hysteresis loops to the evolution of the microstructure. To do that, we have plotted the ratio of the remnant magnetization (M_{rem}) and the magnetization at 12.5 kOe ($M_{12.5\ kOe}$) for the perpendicular hysteresis loops, $M_{rem}/M_{12.5\ kOe}$, as a function of the ratio between the intensity of the (113) diffraction peak of the $TbFe_2$ (I_{TbFe2}) and the (110) peak of FeGa (I_{FeGa}), I_{TbFe2}/I_{FeGa}. It is clear from figure 4b that the OOP component of the magnetization increases as a microstructure closer to the $TbFe_2$ is developed upon the increase of Tb in the compound.

We can further analyze the evolution of the microstructure by means of FC curves. In materials systems comprised of heavy rare earths and magnetic transition metals it is observed a zero or a minimum value for the magnetization in the FC curves, generally denoted as the Compensation temperature (T_{Comp}), due to the antiferromagnetic coupling between these two type of atoms [34]. The presence of T_{Comp} in our samples can only be due to the existence of Tb-Fe alloys and thus, it can be used to obtain information about them. Nevertheless, it is important to consider that the presence of any other ferromagnetic phase in the ternary compound has an additional effect on the magnetization curve. In the FC curves of our samples we observe a minimum or a change of slope that marks the position of the T_{Comp} (Fig. 5a) and we can infer information about Tb-Fe alloys from it. A not clear compensation point indicates the presence of another magnetic phase that in these compounds is related to Fe-Ga alloys. In any case, the T_{Comp} is only due to the Tb-Fe alloys being possible to qualitatively determine their composition because the lower the T_{Comp}, the lower the Tb content [35]. Therefore, the shift of the T_{Comp} from 11 K to around 150 K shows the Tb

enrichment of the Tb-Fe phase present in the samples in agreement with the evolution of the microstructure towards one closer to the $TbFe_2$ as observed by XRD (Figure 1). We have also performed hysteresis loops at low temperature (10 K). The coercivity in the layer with the highest Tb content is much higher with respect to the alloy with the lowest (fig. 5b). This increase of coercivity can be taken as a further indication of a structure close to the $TbFe_2$ in the ternary compound with the highest Tb content as $TbFe_2$ exhibits a much higher coercivity than Fe-Ga [36]. Therefore, the growth conditions proposed in this work enable to obtain an OOP component of the magnetization in Tb-Fe-Ga thin films comprised of two separate phases. Nevertheless, it is enhanced as a microstructure closer to the $TbFe_2$ is developed upon the increase of Tb doping.

4. Conclusions

We have grown $Tb_xFe_{73}Ga_{27-x}$ (7 at.% ≤ x ≤ 11 at.%) thin films by cosputtering from two targets with composition $Tb_{33}Fe_{67}$ and $Fe_{72}Ga_{28}$, respectively. The growth conditions used here, DC power sources in the two targets and a lower target to substrate distance, in comparison to previous works have enabled us to tune the microstructure of the ternary compounds from two to one structural phase as the Tb content is increased. Although PMA has not been obtained in none of the samples, we have observed by MFM a significant OOP component of the magnetization stable up to external magnetic fields of 800 Oe. This magnetic signal is measured even in layers that exhibit two structural phases being enhanced upon the increase of Tb doping. Experimental results indicate that this can be due to the development of a microstructure closer to the $TbFe_2$.

Acknowledgements. We thank 'CAI Difracción de rayos-X' of UCM for the x-ray diffractometry measurements. This work has been financially supported through the projects PRIN 2010ECA8P3 'DyNanoMag' and FIRB2010 RBFR10E61T 'NANOREST' of the Italian Ministry of Education, University and Research and

project of the Universidad Complutense de Madrid ‘Ayudas para Grupos de Investigación GR3/14’.

References

[1] Clark A E, Restorff J B, Wun-Fogle M, Lograsso T A and Schlagel D L 2000 *IEEE Trans Magn* **36** 3238.

[2] Clark A E, Wun-Fogle M, Lograsso T A and Cullen J R 2001 *IEEE Trans Magn* **37** 2678.

[3] Laver M, Mudivarthi C, Cullen J R, Flatau A B, Chen W-C, Watson S M and Wuttig M 2010 *Phys Rev Lett* **105** 027202.

[4] Ruffoni M P,. Pascarelli S, Grössinger R, Sato Turtelli R, Bornio-Nunes C and Pettifer R F 2008 *Phys. Rev. Lett.* **101** 147202.

[5] Cao H, Gehring P M, Devreugd C P, Rodriguez-Rivera J A, Li J and Viehland D 2009 *Phys. Rev. Lett.* **102** 127201.

[6] Arenholz E, van der Laan G, McClure A and Idzerda Y 2010 *Phys. Rev. B* **82** 180405.

[7] Ikeda O, Kainuma R, Ohnuma I, Fukamichi K and Ishida K 2002 *J. Alloys Compnd.* **347** 198.

[8] Xing Q, Du Y, McQueeney R J and Lograsso T A 2008 *Acta Materialia* **56**, 4536.

[9] Cao H, Bai F, Li J, Viehland D D, Lograsso T A and Gehring P M 2005 *J. Alloys Compnd.* **465** 244.

[10] Barturen M, Rache Salles B, Schio P, Milano J, Butera A, Bustingorry S, Ramos C, de Oliveira A J A, Eddrief M, Lacaze E, Gendron F, Etgens V H and Marangolo M 2012 *Appl. Phys. Lett*. **101** 092404.

[11] Reddy S M, Park J J, Na S M, Maqableh M M, Flatau A. B and Stadler B J H 2011 *Advanced Functional Materials* **21** 4677.

[12] Iselt D, Gaitzsch U, Oswald S, Fähler S, Schultz L and Schlörb H 2011 *Electrochim. Acta* **56** 5178.

[13] Dunlap R A, Deschamps N C, Mar R E and Farrell S P 2006 *J. Phys.: Conden. Matter*. **18** 4907.

[14] Basantkumar R R, Stadler B J H, Robbins W P and Summers E M 2006 *IEEE Trans. Magn.* **42** 3102.

[15] Ranchal R and Maestre D 2014 *J. Phys. D: Appl. Phys.* **47** 355004.

[16] Clark A E and Belson H S 1972 *Phys Rev B* **5**:3642.

[17] Harris V G, Aylesworth K D, Das B N, Elam W T and Koon N C 1992 *Phys Rev Lett* **69** 1939.

[18] Hellman F and Gyorgy E M 1992 *Phys Rev Lett* **68** 1391.

[19] Ranchal R, López E, Prieto J L and Aroca C 2011 *Acta Mater* **59** 2865.

[20] Ma T, Hu S, Bai G, Yan M, Lu Y, Li H, Peng X and Ren X 2015 *Appl Phys Lett* **106** 112401.

[21] Wu W, Liu J H, Jiang C B, Xu H B 2013 *Appl Phys Lett* **103** 262403.

[22] Jiang L, Yang J, Hao H, Zhang G, Wu S, Chen Y, Obi O, Fitchorov T and Harris V G 2013 *Appl Phys Lett* **102** 222409.

[23] Fitchorov T I, Bennet S, Jiang L, Zhang G, Zhao Z, Chen Y and Harris V G 2014 *Acta Mater* **73** 19.

[24] Ranchal R and Gutiérrez-Díez V 2013 *Thin Solid Films* **534** 557.

[25] Ranchal R, Fin S, Bisero D and Aroca C 2014 *J Alloys Compnd* **582** 839.

[26] Ranchal R and Maestre D 2014 *J Phys D: Appl Phys* **47** 355004.

[27] Madami M, Bisero D, Gubbiotti G, Tacchi S, Carlotti G, Nakano K and Ono T 2012 *IEEE Trans Magn* **48** 1269.

[28] Sepioni M, Madami M, Tacchi S, Gubbiotti G, Carlotti G, Bisero D, Adeyeye A O, Singh N and Goolaup S 2010 *J Phys: Conf Ser* **200** 072089.

[29] Eberl C, Liese T, Schlenkrich F, Döring F, Hofsäss H and Krebs H U 2013 *App. Phys A* **111** 431.

[30] Zhou X W and Wadley H N G 1999 *Surf Sci* **431** 58.

[31] Tacchi S, Fin S, Carlotti G, Gubbiotti G, Madami M, Barturen M, Marangolo M, Eddrief M, Bisero D and Rettori A 2014 *Phys Rev B* **89** 024411.

[32] Gubbiotti G, Malagò P, Fin S, Tacchi S, Giovannini L, Bisero D, Madami M, Carlotti G, Ding J, Adeyeye A O and Zivieri R 2014 *Phys Rev B* **90** 024419.

[33] Ranchal R, Fin S and Bisero D 2015 *J Phys D: Appl Phys* **48** 075001.

[34] Camley R E and Stamps R L 1993 *J Phys Condens Matter* **5** 3727.

[35] Mimura Y, Imamura N, Kobayashi T, Okada A and Kushiro A 1978 *J Appl Phys* **49** 1208.

[36] Clark A E 1973 *Appl Phys Lett* **23** 642.

Table caption.

Table I. Summary of growth conditions and composition of the samples studied in this work.

Table I

Composition	Growth conditions
$Tb_7Fe_{73}Ga_{20}$	$TbFe_2$. DC: 50 W Fe_3Ga. DC: 90 W
$Tb_8Fe_{73}Ga_{19}$	$TbFe_2$. DC: 60 W Fe_3Ga. DC: 90 W
$Tb_{10}Fe_{73}Ga_{17}$	$TbFe_2$. DC: 70 W Fe_3Ga. DC: 90 W
$Tb_{11}Fe_{73}Ga_{16}$	$TbFe_2$. DC: 90 W Fe_3Ga. DC: 90 W

Figure captions

Figure 1. X-ray diffraction scans of ternary compounds with different composition and a Mo layer. The composition is displayed in each curve and the curves are vertically shifted for clarity. (a) θ-2θ complete scan, and (b) detail of the area of interest. The position of the $TbFe_2$(113) and α-Fe(110) are marked with a dashed and dotted line, respectively.

Figure 2. Comparison of (□) in-plane and (•) out-of-plane hysteresis loops recorded at room temperature for layers with different composition, (a) $Tb_7Fe_{73}Ga_{20}$ and (b) $Tb_{11}Fe_{73}Ga_{16}$. The insets of (a) and (b) show the low field region in detail. In the two graphs the hysteresis loops are normalized to the value of the magnetization at 12.5 kOe.

Figure 3. (a) MFM image at remanence of the sample with a Tb content of 10 at.% and (b) corresponding AFM topography. The circles and ellipses indicate particular regions where the MFM signal reaches peaks of intensity or a particular morphology is observable: in the same subareas, the AFM image is clearly uncorrelated from the MFM signal. In (c) we report the Power Spectral Density from which the average size of magnetic domains is calculated to be greater than 50 nm. In (d) there is a section of the topography which shows that highest surface peaks (10 nm) are very low compared to the lift scan heigh (80 nm) and comparing it with the corresponding MFM profile (e) the differencies are clear. The results must be considered as representative of the magnetic signal observed in all the analyzed samples.

Figure 4. (a) Detail of the perpendicular hysteresis loops for layers with different composition: (□) $Tb_7Fe_{73}Ga_{20}$, (■) $Tb_8Fe_{73}Ga_{19}$, (○) $Tb_{10}Fe_{73}Ga_{17}$, and (•) $Tb_{11}Fe_{73}Ga_{16}$. (b) Ratio between the remnant magnetization and the magnetization at 12.5 kOe ($M_{rem}/M_{12.5\ kOe}$) measured in the perpendicular hysteresis loops as a function of the intensity of the diffraction peak of the (113) reflection of the $TbFe_2$ and the (110) of FeGa (I_{TbFe2}/I_{FeGa}). The dotted line is a guide to the eye.

Figure 5. (a) FC curves of two ternary compounds (■) $Tb_8Fe_{73}Ga_{19}$ and (•) $Tb_{11}Fe_{73}Ga_{16}$. The inset is a detail of the low temperature range to better show the T_{Comp} of the $Tb_8Fe_{73}Ga_{19}$. (b) Hysteresis loops at 10 K for the (□) $Tb_7Fe_{73}Ga_{20}$ and (•) $Tb_{11}Fe_{73}Ga_{16}$ compounds. Inset: Complete hysteresis loops. The hysteresis loops are normalized to the value of the magnetization at 50 kOe.

Figure 1. **R. Ranchal et al**

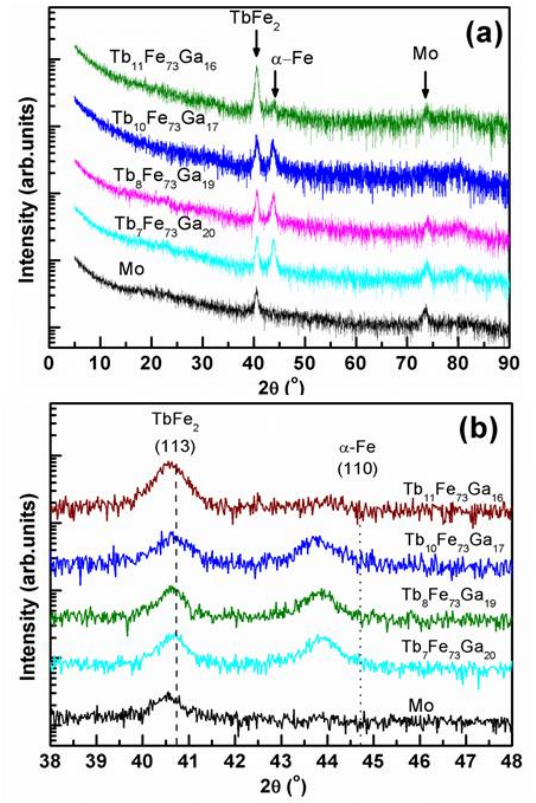

Figure 2. **R. Ranchal et al**

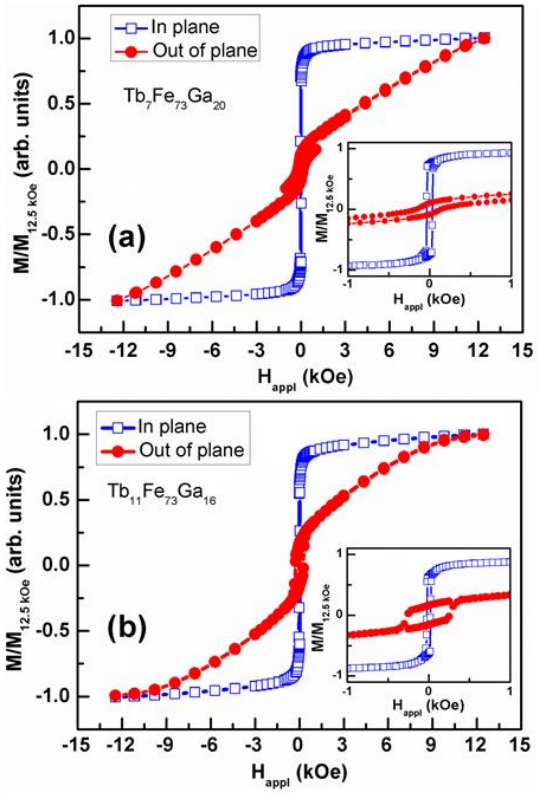

Figure 3. **R. Ranchal et al**

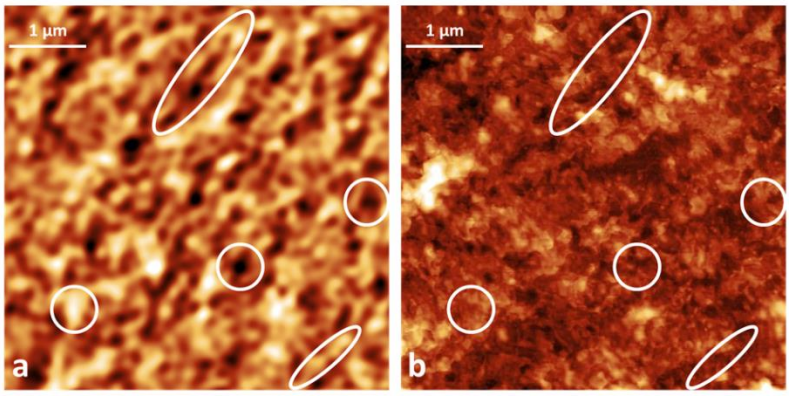

Figure 4. **R. Ranchal et al**

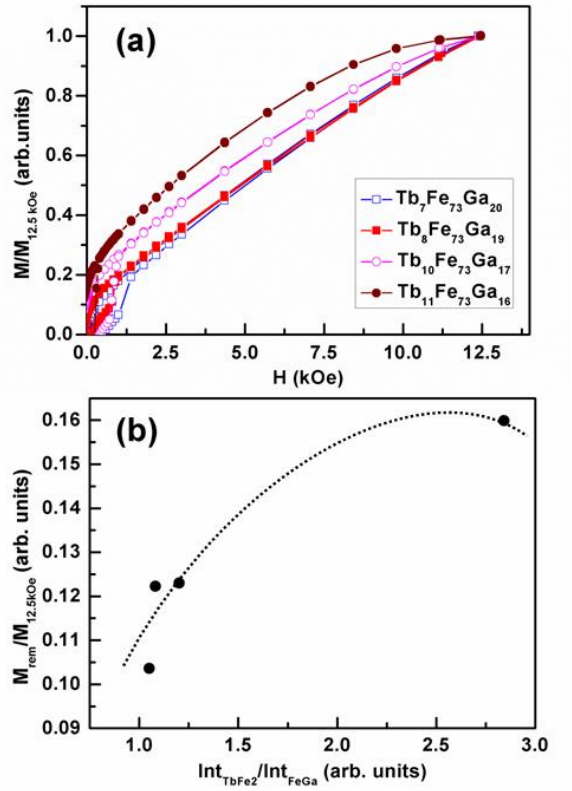

Figure 5. **R. Ranchal et al.**